Magnetic Reconnection and Plasma Dynamics in Two-Beam Laser-Solid Interactions

P. M. Nilson,[1] L. Willingale,[1] M. C. Kaluza,[1,*] C. Kamperidis,[1] S. Minardi,[2] M. S. Wei,[1,†] P. Fernandes,[1] M. Notley,[3] S. Bandyopadhyay,[3] M. Sherlock,[3] R. J. Kingham,[1] M. Tatarakis,[2] Z. Najmudin,[1] W. Rozmus,[4] R. G. Evans,[3] M. G. Haines,[1] A. E. Dangor,[1] and K. Krushelnick[1]

[1]*Department of Physics, Imperial College, London SW7 2AZ, United Kingdom*
[2]*Technological Educational Institute of Crete, Chania, Crete, Greece*
[3]*Central Laser Facility, Rutherford Appleton Laboratory, Chilton, Didcot, Oxon., United Kingdom*
[4]*Department of Physics, University of Alberta Edmonton, Alberta, Canada*

(Received 22 May 2006; published 19 December 2006)

We present measurements of a magnetic reconnection in a plasma created by two laser beams (1 ns pulse duration, 1×10^{15} W cm^{-2}) focused in close proximity on a planar solid target. Simultaneous optical probing and proton grid deflectometry reveal two high velocity, collimated outflowing jets and 0.7—1.3 MG magnetic fields at the focal spot edges. Thomson scattering measurements from the reconnection layer are consistent with high electron temperatures in this region.

DOI: 10.1103/PhysRevLett.97.255001 PACS numbers: 52.38.Fz, 52.30.−q, 52.35.Vd, 52.50.Jm

Plans for achieving ignition by inertial confinement on the National Ignition Facility and the Laser Mégajoule will use a hohlraum-generated, temporally shaped radiation drive to implode a deuterium-tritium pellet. The thermal radiation drive is generated by focusing multiple laser beams in close proximity to each other on the inner surface of a high-Z hohlraum cavity [1].

A detailed knowledge of the hohlraum plasma evolution is required for improving hohlraum design and for benchmarking multidimensional radiation hydrodynamic codes. Magnetic fields are often important for electron energy transport [2] in such experiments but, until recently, have largely been ignored and have proven difficult to implement into existing codes. Experimental benchmarking data is required, and consequently there is much interest in spatially resolved measurements of the evolution of hot (>1 keV) and dense ($n_e > 10^{19}$ cm^{-3}) plasmas. Schemes investigated include laser-exploded foils [3,4] and the convergent flows from conical [5] and cylindrical targets [6].

In this Letter, we present measurements of the plasmas created by closely focusing two heater beams on a planar foil target. The two plasmas typically collide and stagnate, yet for laser spot separations of greater than about seven focal spot diameters, the sudden appearance of two very distinct, highly collimated jets can be observed. The azimuthal $\nabla T_e \times \nabla n_e$ magnetic fields that are generated around each laser spot [7] have also been observed using proton deflectometry. These measurements reveal plasma dynamics and a magnetic field distribution in accordance with a reconnection geometry.

During reconnection, two counterstreaming plasmas meet, and the local diffuson of a magnetic field within a neutral current sheet allows field lines to break and reconnect [8]. Some fraction of the magnetic energy is converted into thermal energy as the system relaxes to a lower energy state and reorganizes its field line topology [9,10]. Several theories have identified the important role of field-aligned outflowing jets in energy conservation. However, many details of the acceleration and heating mechanisms remain unknown. In our experiment, Thomson scattering measurements in the reconnection layer reveal high electron temperatures of 1.7 keV. Such high electron temperatures are in contrast to the high ion temperatures that are more consistent with a hydrodynamically stagnating plasma in the absence of magnetic fields [11,12]. The experimentally observed plasma flows and magnetic field convection, high electron temperatures, and jet formation are consistent with a magnetic reconnection.

The experiment used the Vulcan laser at the Rutherford Appleton Laboratory, UK. The experiment is shown in Fig. 1. Two heater beams, with wavelength $\lambda = 1.054$ μm, irradiated either an aluminum or gold target foil. A 1 ns duration square pulse was used with an average energy of 200 J per heater beam. The targets were 3 mm × 5 mm foils of 20–100 μm thickness. Each beam was focused using $f/10$ optics to a focal spot diameter of 30–50 μm FWHM, giving an incident laser intensity of 1×10^{15} W cm^{-2}. The two heater beams were aligned with varying on-target separations.

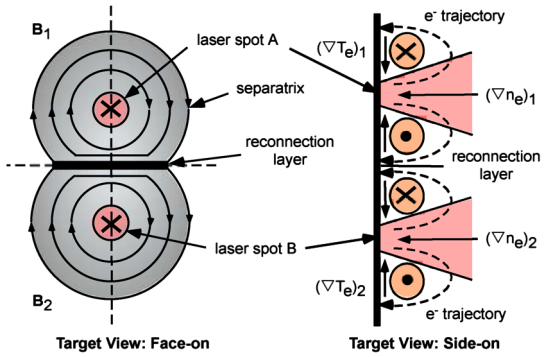

FIG. 1 (color online). The target geometry and field configurations.

The target plasma was diagnosed with multiple diagnostics. Firstly, a 10 ps pulse duration, 263 nm probe beam was passed transverse to the target surface at various times. Probe beam light refracted by the target plasma was reimaged and divided into two diagnostic channels with a magnification of 13 and a resolution of 5 μm. Shadowgraphy was used to monitor the global plasma dynamics, while the plasma electron density was measured using a modified Nomarski interferometer. A combination of reflective and bandpass ($\Delta\lambda = 10$ nm) interference filters was used to reduce the detectable self-emission from the target.

Shadowgrams of aluminum interactions are shown in Figs. 2(a) and 2(b). For laser spot separations of around 200 μm in Fig. 2(a), a quasihomogenous plasma is observed at $t = t_0 + 2.0$ ns, where the heater beams turn on at t_0. The darker areas correspond to regions which are opaque to the probe light and also regions where there are large density gradients. Figure 2(b) demonstrates the surprising result that upon separating the laser spots to around 400 μm, a very prominent, high velocity flow of plasma is created from the midplane, propagating at $v_\perp \approx 5 \times 10^7$ cm s^{-1} away from the target surface. This image was taken at $t = t_0 + 1.5$ ns.

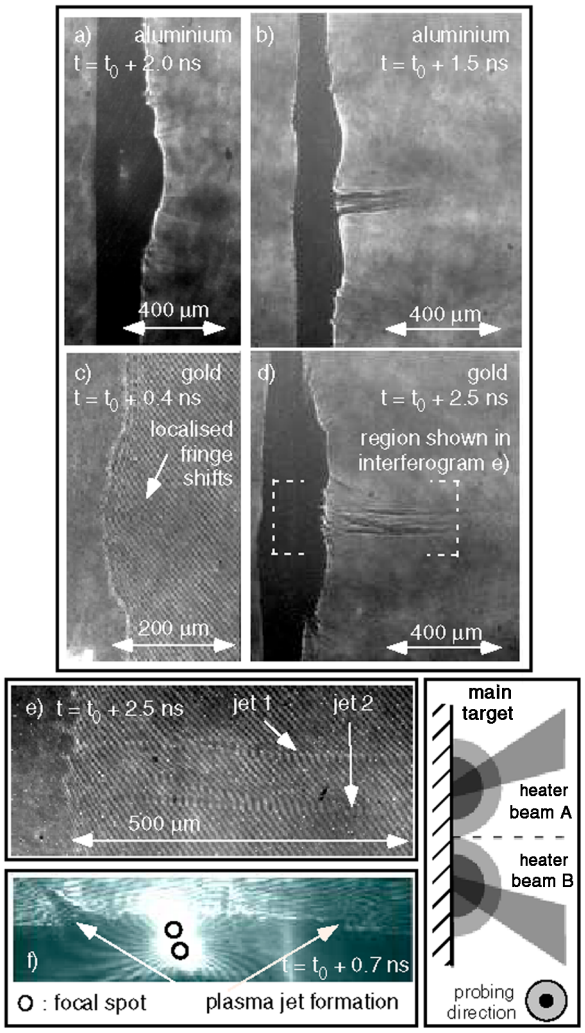

FIG. 2 (color online). Transverse 263 nm probe beam images of aluminum targets (a, b) and gold targets (c–f). The probe beam geometry is shown (lower right).

Similar dynamics are observed in gold interactions, as shown in Figs. 2(c) and 2(d), with laser spot separations of around 400 μm. Figure 2(c) is an interferogram of the midplane taken at $t = t_0 + 0.4$ ns, showing the first low density interaction between the laser ablated plasmas following a finite transit time from each laser spot. Figure 2(d) is a shadowgram taken at $t = t_0 + 2.5$ ns and shows the subsequent jet formation. A simultaneous interferogram is shown in Fig. 2(e). The central plasma feature is not a stagnation column but the transverse projection of two high velocity jets. Localized fringe shifts identify the two highly collimated jets. They exhibit great symmetry and extend over 400 μm from the target surface and have an electron density of around 6×10^{19} cm^{-3}. Radiation losses in the gold target has produced more collimated flows in comparison to the aluminum target. Further evidence for the early formation of the two jets comes from viewing the interaction at 90° such that both jets are clearly seen separated [Fig. 2(f)].

The sudden appearance of two distinct jets from the midplane is an important observation and an unexpected result if only hydrodynamics were considered. Once the plasma generated from one laser spot has reached the midplane, its dynamics are influenced by the presence of the plasma generated by the other laser spot. Here there will be a conversion of streaming ion kinetic energy into ion thermal energy where the two flows stagnate and thermalize. Increasing the laser spot separation not only alters the collisionality of the interaction at the midplane, but also the competition between the thermal plasma pressure $n_e k_B T_e$ and the magnetic pressure $B^2/2\mu_0$ in this region. The thermal plasma pressure will reduce here as the laser spot separation increases. The plasma dynamics at the midplane will become increasingly sensitive to the azimuthal $\nabla T_e \times \nabla n_e$ self-generated magnetic fields that are convected into this region through the lowering of the plasma-β (i.e., the ratio of thermal and magnetic pressures).

To further study the magnetostatic and electrostatic field effects, face-on proton grid deflectometry [13] was performed. The protons were derived from a 20 μm thick gold foil located 2 mm behind the main target. A high-intensity, 1 ps pulse duration beam, with an energy of 100 J, was focused onto the gold foil using an $f/3.5$ off-axis parabolic mirror. A peak intensity of 5×10^{19} W cm^{-2} was achieved with a focal spot of 8–10 μm FWHM, containing 30–40 per cent of the energy.

Typical deflectometry data are shown in Fig. 3 for aluminum target interactions. By $t_0 + 100$ ps, protons have been radially deflected away from each of the focal spots by the azimuthal magnetic fields. Proton density perturbations in the focal regions are caused by the localized electric and magnetic fields associated with fine-scale filamentary structures at the target surface. A region of

proton accumulation is observed between the two focal spots, consistent with the azimuthal magnetic fields deflecting protons into the region of magnetic field null.

By $t_0 + 500$ ps, the magnetic fields generated in the plasma have expanded across the target surface at around 10^7 cm s^{-1} and started to interact with each other and form a reconnection geometry (as shown schematically in Fig. 1). At later times, the thin interaction region of around 100 μm thickness develops instabilities, characteristic of the azimuthal magnetic fields, counterstreaming flows, and velocity shear present. It is clear that the plasma is magnetized and the presence of the magnetic field is greatly affecting the plasma dynamics.

The dominant electric field is in the target normal direction $\hat{\mathbf{E}} = E\hat{\mathbf{z}}$; therefore, the protons are deflected by the $\hat{\mathbf{v}} \times \hat{\mathbf{B}}$ force. The proton flux has a range of energies and experiences the magnetic field over some characteristic length L_B depending on the probing time after t_0. For $L_B \approx 100$ μm at $t = 100$ ps, an apparent grid deflection on the film of 500 μm (for protons of 13.5 MeV) indicates a magnetic field of around 1.3 MG. Such conditions and the range of imaged grid deflections around the laser focal spot edges indicate magnetic fields in the range 0.7–1.3 MG at $t = t_0 + 100$ ps.

Thomson scattering (TS) was used to measure the electron temperature in the aluminum interactions. Fig. 4(a) shows the two locations where TS light was collected on different shots using a 10 J, 263 nm probe beam of 1 ns (square) pulse duration. The probe beam was aligned parallel to the target surface and focused to 50 μm using $f/10$ optics. The length of the cylindrical scattering volume was approximately 70 μm. Scattered light was collected at $\theta = 90°$ and reimaged with a magnification of 1.5 onto a 100 μm spectrometer slit. The signal was spectrally dispersed using a 3600 lines/mm grating and a 1 m spectrometer coupled to a streak camera. The time-resolved TS spectra were measured with a temporal resolution of 100 ps and a wavelength resolution of 0.05 nm.

Figure 4(b) shows a TS spectrum from scattering volume 1. For $t_0 + 1.0$ ns $< t < t_0 + 2.0$ ns, two ion acoustic features are observed. Their separation reduces in time, indicating a decreasing electron temperature from hydrodynamic expansion. Figs. 4(c) and 4(d) show the spectra at $t = t_0 + 1.5$ ns and $t = t_0 + 2.25$ ns with theoretical fits that have been obtained from standard collisionless theory of the dynamical form factor [14]. The electron and ion velocity distribution functions are Maxwellians, the electron density is $n_e = 5 \times 10^{19}$ cm^{-3}, and the fits include experimental broadening due to the wavelength resolution of 0.05 nm. The separation between the two ion acoustic resonances in Figs. 4(c) and 4(d) are consistent with electron temperatures of 800 eV and 700 eV, respectively. The slight asymmetry in the ion acoustic peaks in Fig. 4(d) is

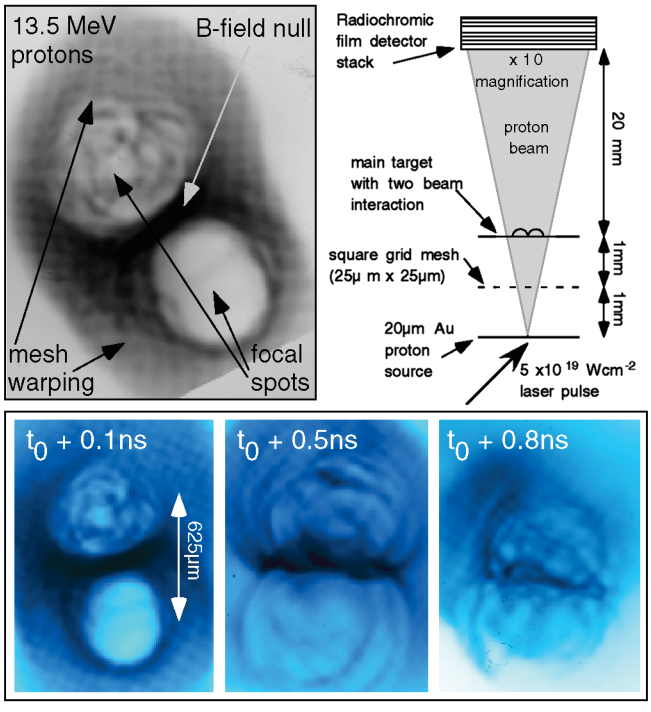

FIG. 3 (color). Proton grid deflectometry images of aluminum target interactions taken 100 ps, 500 ps, and 800 ps after the heater beams arrive at the target surface. Each image is shown for protons with an energy of $E_P = 13.5$ MeV.

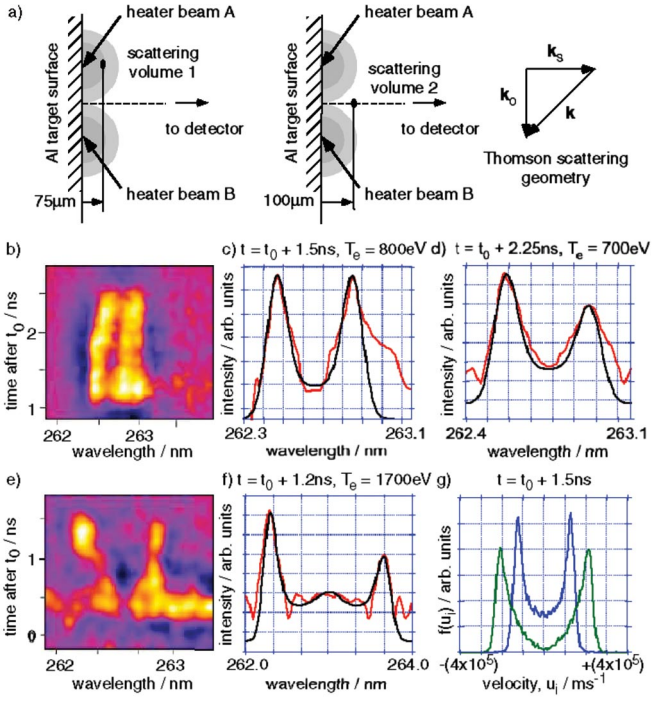

FIG. 4 (color). The scattering geometry (a) and the TS spectra from scattering volumes 1 (b, c, d) and 2 (e, f). The spectra are compared with standard theoretical fits [14] (c, d). A spectrum from the reconnection region is shown in (e) and compared in (f) to the spectrum predicted using the ion distribution function (IDF) shown in (g) (blue curve). This IDF is calculated using a hybrid kinetic ion and fluid electron code [15]. See text for details.

modeled by an electron drift velocity of 3.0×10^7 cm s^{-1}. Such a drift of the bulk electrons may occur in response to the heat flux carried by fast particles.

Figure 4(e) shows a TS spectrum from scattering volume 2. Electrons are not directly heated by the laser beams in this region. A large increase in the ion acoustic peak separation for $t > t_0 + 1.0$ ns is observed. For an equilibrium plasma, a straightforward fit of the experimental scattering spectrum at $t = t_0 + 1.2$ ns in Fig. 4(f) would result in an electron temperature of 9 keV. X-ray pinhole imaging confirmed the presence of plasma heating at the midplane; however, such temperatures are unphysically high, particularly since the plasma in volume 2 has to expand into this region from the laser heated coronas (volume 1) where the temperature was measured at 700–800 eV.

To understand the plasma conditions in volume 2, we have performed 2D simulations using a hybrid code [15] with kinetic ions and fluid electrons. The measured plasma parameters from volume 1 provided boundary conditions within two laser spots. Transverse plasma expansion results in two counterstreaming ion populations as described by the calculated ion distribution functions (IDFs) in Fig. 4(g). The green curve is the spatially integrated IDF as a function of the velocity along the line joining the two laser spots, while the blue curve is a function of the velocity along the TS diagnostic viewing angle. We have included such an IDF (blue curve), i.e., the sum of two shifted Maxwellians, in the calculation of the TS spectrum at $t = t_0 + 1.2$ ns, as shown in Fig. 4(f). A very good fit to the experimental data has been obtained for an electron temperature $T_e = 1.7$ keV ($T_e = T_i$, $n_e = 2.5 \times 10^{20}$ cm^{-3}) and the ion flow velocity $u_i = 2.0 \times 10^7$ cm s^{-1} which is on the order of the sound velocity. These two resonances are the result of four ''beamlike'' ion modes in the plasma caused by interpenetrating flows [16] that will be present post-reconnection.

Such electron temperatures are surprisingly high since there is no direct laser heating in this region. If the midplane interaction consisted of a standard collision, it would be ion heating that dominated the interaction [11,12]. The electrons gain energy subsequently through electron-ion equilibration. However, the time scale over which this occurs is many nanoseconds. We measure high electron temperatures that cannot be reconciled to electron-ion equilibration alone or compressional heating (this is not an efficient plasma compression geometry). This therefore indicates another energy source. Such a source would need to supply energy to the electrons at a sufficiently high rate that it was not simply radiated away. The only source available with sufficient free energy that could be provided at such a rate is the conversion of magnetic energy into plasma thermal energy through a reconnection mechanism.

The present interaction can be compared to the Sweet-Parker (SP) model of magnetic reconnection [17,19]. For aluminum plasmas, the Alfvén velocity $v_A = 1.35 \times 10^7$ cm s^{-1}, the Alfvén transit time $\tau_A = L_H/v_A = 7.4 \times 10^{-10}$ s, and the resistive diffusion time scale $\tau_R = \mu_0 L_H^2/\eta_\perp = 2.2 \times 10^{-8}$ s, assuming $L_H = 100$ μm, $T_e = 800$ eV, and $B = 1$ MG. Here, the perpendicular Spitzer resistivity $\eta_{\text{perp}} = 2\eta_\parallel$ is used because the current flows perpendicular to the field. The SP reconnection rate is given by $(\tau_R \tau_A)^{1/2} = 4$ ns. However, such estimates are subject to significant uncertainty. L_H could be tens of microns in the reconnection region and reduce the calculated reconnection rate to around 0.5 ns. The SP model has also been shown not to be universally applicable, such as in solar flares [20], for example, where the predicted reconnection rate is orders of magnitude too slow. Further study is required to confirm the validity of the SP model in this case.

In summary, we have studied a magnetic reconnection geometry created in a laser-produced plasma. The magnetic fields, plasma flows, field convection, jet formation, and high electron temperatures (for relatively large laser spot separations, in which the magnetic pressure will become increasingly important at the midplane) are consistent with a magnetic reconnection rather than a standard hydrodynamic collision in the absence of magnetic fields. Such interaction geometries may help in elucidating the microphysics and heating mechanisms during magnetic reconnection.

The authors acknowledge the assistance of the CLF staff and the support of the UK Engineering and Physical Sciences Research Council and AWE plc, Aldermaston, UK.

*Present address: Institute for Optics and Quantum Electronics, Germany.
†Present address: Center for Energy Research, University of CA, USA.

[1] J. D. Lindl *et al.*, Phys. Plasmas **11**, 339 (2004).
[2] P. Nicolai *et al.*, Phys. Plasmas **7**, 4250 (2000).
[3] R. L. Berger *et al.*, Phys. Fluids B **3**, 3 (1991).
[4] P. W. Rambo *et al.*, Phys. Plasmas **1**, 4050 (1994).
[5] D. R. Farley *et al.*, Phys. Rev. Lett. **83**, 1982 (1999).
[6] S. H. Glenzer *et al.*, Phys. Rev. Lett. **79**, 1277 (1997).
[7] J. A. Stamper *et al.*, Phys. Rev. Lett. **40**, 1177 (1978).
[8] D. Biskamp, Phys. Rep. **237**, 179 (1994).
[9] T. D. Phan *et al.*, Nature (London) **439**, 175 (2006).
[10] H. Ji *et al.*, Phys. Rev. Lett. **80**, 3256 (1998).
[11] O. Rancu *et al.*, Phys. Rev. Lett. **75**, 3854 (1995).
[12] C. Chenais-Popovics *et al.* Phys. Plasmas **4**, 190 (1997).
[13] A. J. Mackinnon, Rev. Sci. Instrum. **75**, 3531 (2004).
[14] J. Sheffield, *Plasma Scattering of Electromagnetic Radiation* (Academic, New York, 1975).
[15] M. Sherlock *et al.*, Phys. Plasmas **11**, 1609 (2004).
[16] L. V. Powers and R. L. Berger, Phys. Fluids **31**, 3109 (1988).
[17] P. A. Sweet, in *Electromagnetic Phenomena in Cosmical Physics*, edited by B. Lehnert (Cambridge University Press, New York, 1958) p. 123.
[18] E. N. Parker, J. Geophys. Res. **62**, 509 (1957).
[19] R. M. Kulsrud, *Plasma Physics for Astrophysics* (Princeton University Press, Princeton, NJ, 2004).
[20] M. G. Kivelson and C. T. Russell, *Introduction to Space Physics* (Cambridge University Press, Cambridge, England, 1995), and references therein.